ACS APPLIED MATERIALS & INTERFACES

Research Article

www.acsami.org

Intracellular Degradable Hydrogel Cubes and Spheres for Anti-Cancer Drug Delivery

Bing Xue,[†,⊥] Veronika Kozlovskaya,[†,⊥] Fei Liu,[†] Jun Chen,[†] J. Fox Williams,[†] Javier Campos-Gomez,[‡] Mohammad Saeed,[‡] and Eugenia Kharlampieva*[,†,§]

[†]Department of Chemistry and [§]Center of Nanoscale Materials and Biointegration, University of Alabama at Birmingham, Birmingham, Alabama 35294, United States

[‡]Department of Biochemistry and Molecular Biology, Southern Research Institute, Drug Discovery Division, Birmingham, Alabama 35205, United States

Supporting Information

ABSTRACT: Shape and responsiveness of nanoengineered delivery carriers are crucial characteristics for rapid and efficient delivery of therapeutics. We report on a novel type of micrometer-sized hydrogel particles of controlled shape with dual pH- and redox-sensitivity for intracellular delivery of anticancer drugs. The cubical and spherical poly(methacrylic acid) (PMAA) networks with disulfide links are obtained by cross-linking PMAA with cystamine within hydrogen-bonded multilayers of PMAA/poly(vinylpyrrolidone) (PMAA/PVPON) on sacrificial mesoporous templates. The pH-triggered hydrogel swelling/shrinkage not only affords effective doxorubicin entrapment but also efficient endosomal/lysosomal escape, and redox-triggered degradation provides drug release into the cytosolic space. The hydrogels degrade rapidly to low molecular weight chains in the presence of the typical intracellular concentration of glutathione, which should ensure a rapid renal clearance in vivo. Particle shape is found to affect internalization at the initial step of cell-particle interactions. Drug-loaded spherical particles are found to be 12% more cytotoxic than the corresponding cubes within the first 10 h of cell incubation suggesting more rapid internalization of spheres. Both doxorubicin-loaded hydrogel cubes and spheres demonstrate 50% and 90% cytotoxicity when incubated with HeLa cancer cells for 24 and 48 h, respectively. The presented approach integrates the advantages of pH-sensitivity, enzymatic degradation, and shape-regulated internalization for novel types of "intelligent" three-dimensional networks with programmable behavior for use in controlled delivery of therapeutics.

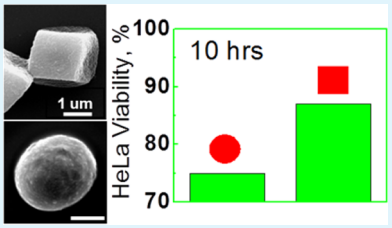

KEYWORDS: *particle shape, multilayer hydrogel, pH-responsive, intracellular degradable, poly(methacrylic acid)*

INTRODUCTION

The design of smart polymeric systems for intracellular therapeutic delivery helps resolve the problematic issues associated with delivery of unmodified chemotherapeutics including poor solubility and limited stability in plasma, inefficient intracellular delivery, multidrug resistance, non-selective toxicity, and a short circulation lifetime.[1−5] A variety of polymeric systems including micro- and nanoscale dendrimers, micelles, polymersomes, multilayer capsules, and hydrogel particles have been developed as smart drug delivery vehicles.[6−10] Among those, stimuli-responsive systems have drawn extensive attention because of the in-built capabilities for a triggered drug release using a particular stimulus such as intracellular acidic pH, elevated temperature, and reductive environment at the pathological site.[11−13] Stimuli-responsive hydrogel systems display such important characteristics as reversible volume transformations and controlled drug release.[14,15] Their stimuli-triggered volume changes[16] along with good biocompatibility and biodegradability[17,18] can be used for tumor targeting by anchoring the vehicles in the tumor tissue upon their size increase and enabling the release of encapsulated therapeutics.

The redox response is the most appealing property that can be imparted on the intracellular drug delivery vehicle due to a significant difference in the redox potential between intra- and extracellular environments. Glutathione (GSH), a tripeptide enzyme in cells, is able to reduce disulfide bonds to the corresponding thiols as an electron donor.[19] The intracellular GSH concentration of 2−10 mM is 1000 times higher than that of 2−20 μM in the extracellular environment with some tumor cells having GSH concentration several times higher than normal cells.[20] Furthermore, the endosomes/lysosomes contain a high content of the reducing enzyme γ-interferon-lysosomal thiol reductase (GILT), which can reduce protein disulfide bonds at low pH, and of cysteine, which may also exhibit reducing properties.[21] Thus, disulfide-based drug delivery carriers have demonstrated great potential for a rapid intracellular drug release while being stable in the extracellular media, which inhibits the occurrence of drug resistance.[22] Wang and co-workers have produced spherical poly(methacrylic acid)

Received: April 17, 2015
Accepted: June 1, 2015
Published: June 1, 2015

DOI: 10.1021/acsami.5b03360
ACS Appl. Mater. Interfaces 2015, 7, 13633−13644

(PMAA) nanogels with redox- and pH-responsiveness for controlled drug delivery.[23] Caruso and collaborators have been developing spherical degradable hydrogel multilayer capsules based on thiol-modified PMAA for delivery and controlled release of small molecular weight drugs, siRNA, and oligonucleotides.[24−26]

Shape of the drug delivery vehicles was reported to be as important as their surface chemistry and size in affecting drug delivery efficiency.[27−30] Cellular internalization and circulation half-life of the drug carrier can be enhanced with a proper particle shape.[20,19,31−33] For instance, blood circulation time was shown to be extended for PEGylated tobacco mosaic virus with a rod or discoid shape in contrast to samples having a spherical shape.[34] Mitragotri et al. demonstrated that elliptical PLGA discoid rigid particles with an aspect ratio of 5 showed slower endocytosis rates in contrast to spherical ones.[35] We have lately found that rigid hydrogen-bonded tannic acid/poly(*N*-vinylpyrrolidone) (TA/PVPON) hemispherical capsules produced layer-by-layer (LBL) were internalized by macrophages 2 times more efficiently that those of the spherical shape.[32] In our recent work, we also showed that red blood cell mimicking multilayer hydrogel discoidal capsules of PMAA/PVPON interacted differently with J774A.1 macrophages, HMVEC endothelial cells, and 4T1 breast cancer cells and that the discoidal capsules showed 60% lower internalization as compared to spherical capsules.[36]

Despite the crucial role of particle shape in drug delivery, shaped hydrogel systems with environmental responses have been minimally explored.[36,37] The lack of studies in this area is probably associated with the synthetic challenge of integrating stimuli-sensitivity into shaped structures. The paucity of responsive nonspherical hydrogel structures is likely due to their poor mechanical stability.[38] In contrast, the highly cross-linked microsized networks obtained by microfluidics and PRINT offered excellent control over shape and size, but they lacked the capability of dynamic change.[39,40] Apparently, stimuli-triggered dimensional changes of the hydrogel particles require the spatial conditions for polymer chain rearrangement that are not available in particles from those processes.

Our group has recently reported pH-sensitive 2 μm hydrogel cubes comprised of PMAA interconnected networks.[16] Those particles were obtained by sequential infiltration of PMAA and PVPON inside mesoporous manganese oxide templates, followed by cross-linking of PMAA with ethylenediamine and template dissolution.[16] Hydrogel particles afford for high loading capacity provided by the porous interconnected networks,[41,42] a feature challenging to achieve with hydrogel capsules because of drug leakage from the capsule cavity.[43]

In the current study, we report on doxorubicin (DOX)-loaded PMAA hydrogel cubes and spheres capable of both intracellular degradation and pH-responsiveness through introduction of cystamine (CS) cross-links within the networks. The effects of particle shape on GSH-induced degradation, internalization by human cervical carcinoma HeLa cells, and intracellular delivery of DOX are explored. Unlike previous reported spherical thiol-modified PMAA particles swollen only at pH > 6,[10,44] the biodegradable $PMAA_{CS}$ cubical and spherical hydrogels designed herein swell both under neutral and slightly acidic pH conditions. The first swelling (pH > 6) facilitates drug loading within the network, while the second swelling (pH < 6) provides drug release in the early endosomes at pH = 5−6.5[45] or under the slightly acidic pH microenvironment in cancerous tissue.[46] To the best of our knowledge this work is the first example of shaped hydrogels with dual pH- and redox sensitivity. Our approach integrates multistimuli responsiveness into hydrogel particles of nonspherical shape and provides a new strategy to regulate internalization of intracellular responsive drug carriers.

EXPERIMENTAL SECTION

Materials. Poly(methacrylic acid) (PMAA, average M_w 21 800 g mol^{-1}, $Đ$ = 1.32), polyethylenimine (PEI, average M_w 25 000 g mol^{-1}), poly(*N*-vinylpyrrolidone) (PVPON, average M_w 58 000 g mol^{-1}), glycidyl methacrylate (GMA), L-glutathione reduced (GSH), cystamine dihydrochloride, and ethylenediaminetetraacetic acid (EDTA) were purchased from Sigma-Aldrich. 1-Ethyl-3-(3-(dimethylamino)-propyl)-carbodiimide hydrochloride (EDC) was obtained from Chem-Impex International. Ultrapure deionized water with a resistivity of 0.055 μS cm^{-1} was used in all experiments (Siemens). Monobasic sodium phosphate, hydrochloric acid, and sodium hydroxide were from Fisher Scientific. Doxorubicin hydrochloride was purchased from LC Laboratories (USA). Porous cubic (1.5−2 μm) and spherical (1.5−2 μm) Mn_2O_3 microparticles were synthesized as described previously.[16]

Fabrication of Cystamine-Cross-Linked $(PMAAs)_n$ Multilayer Hydrogel Planar Films. Prior to film deposition, Si wafers (University Wafers) were cleaned as described elsewhere.[47] Hydrogen-bonded films of $(PVPON/PMAA)_n$, where subscript *n* denotes the number of deposited polymer bilayers, were built using a dipping LBL assembly. To enhance the surface adhesion of the multilayers, a layer of poly(glycidyl methacrylate) (PGMA) was covalently bound to the wafers first as described previously.[47] The assembly of the (PVPON/PMAA) multilayer was then performed from 0.5 mg mL^{-1} polymer solutions (0.01 M phosphate) followed by CS cross-linking. For that, the carboxyl groups were first activated with water-soluble carbodiimide (5 mg mL^{-1}, 0.01 M phosphate) at pH = 5 for 40 min, followed by exposure to CS (1 mg mL^{-1}, 0.01 M phosphate) at pH = 5.8 for 3 h. PVPON was released from the CS-cross-linked $PMAA_{CS}$ multilayer hydrogel at pH = 8 (0.01 M phosphate) followed by rinsing with pH = 5 (0.01 M phosphate) and gently dried with a stream of nitrogen.

Ellipsometry. Film thickness measurements were performed using an M2000U spectroscopic ellipsometer (Woollam). Dry film measurements were performed between 400 and 1000 nm at 65°, 70°, and 75° angles of incidence. For data interpretation, the ellipsometric angles Ψ and Δ were fitted using a multilayer model composed of Si, SiO_2, and the polymer layer to obtain the film thickness. The SiO_2 thickness was measured for each wafer and was determined using known optical constants. The thickness of the polymer film was obtained by fitting data with the Cauchy approximation. pH-Dependent measurements of the films were performed in situ using a 5 mL liquid flow-through cell (Woollam). The cell was filled with 0.01 M phosphate buffer solution at various pH values, and measurements were taken after 20 min of equilibration. The thickness of the multilayer film at each pH was obtained by fitting data with the Cauchy approximation.[47] GSH-Triggered $PMAA_{CS}$ film degradation was monitored by measuring the change in dry film thickness. For that, $PMAA_{CS}$ multilayer hydrogel films were placed in phosphate buffered saline (PBS, pH = 7.4) and in GSH solution (5 mM, pH = 7.4) at 37 °C. After certain time points, films were taken from the solutions, rinsed with pH = 5 (0.01 M phosphate) three times, and dried under nitrogen. Their dry thickness was measured using ellipsometry.

Synthesis of Biodegradable Cubic and Spherical Microgel Particles. Nanoporous $PMAA_{CS}$ hydrogel particles of cubic and spherical shapes were prepared as described previously.[16] Briefly, hydrogen-bonded $(PMAA/PVPON)_5$ multilayers were assembled LBL inside porous Mn_2O_3 particles that were first exposed to aqueous PEI solution (1.5 mg mL^{-1}) for 1 h. The deposition was performed by sequential exposure of the Mn_2O_3 particles to 1.5 mg mL^{-1} polymer solutions at pH = 3.6 (0.01 M phosphate) with 45 min of deposition time including 15 min of sonication and 30 min of shaking. Then particles were collected by centrifugation at 6000 rpm for 5 min and

DOI: 10.1021/acsami.5b03360
ACS Appl. Mater. Interfaces 2015, 7, 13633−13644

Scheme 1[a]

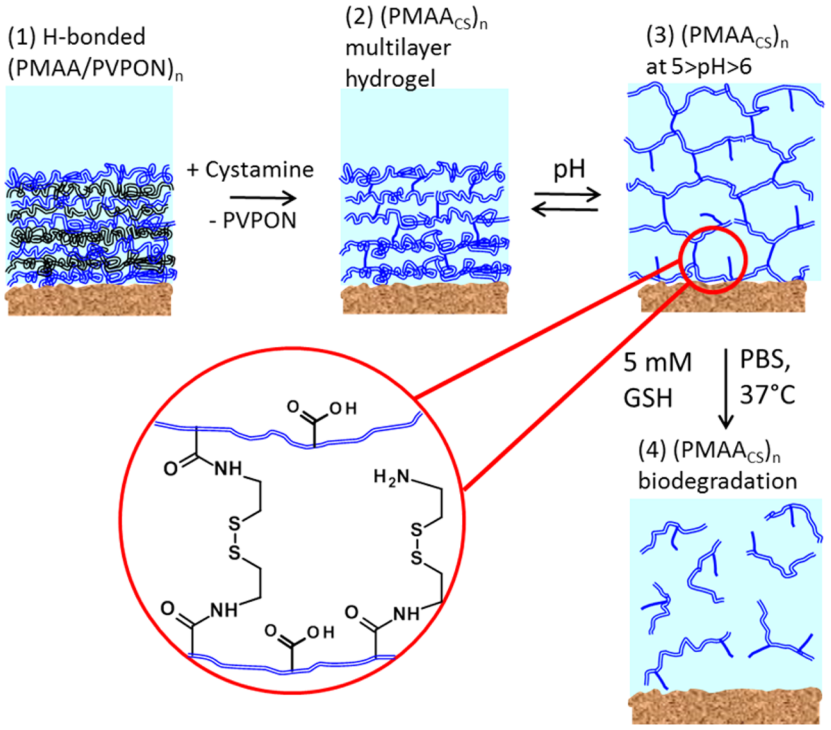

[a]Hydrogen-bonded $(PMAA/PVPON)_n$ multilayer templates (1) were cross-linked with CS to result in a $(PMAA_{CS})_n$ multilayer hydrogel coating (2). This multilayer hydrogel coating swells at pH > 6 (anionic) and pH < 5 (cationic) (3), and is degradable in the presence of GSH due to reduction of disulfide bonds (4).

resuspended in a 0.01 M phosphate at pH = 3.6 to rinse off nonadsorbed polymer. The rinsing was repeated two times. After deposition, the inorganic template was dissolved in 1 M HCl for 24 h followed by six rinses with deionized (DI) water at pH = 2. The PMAA layers were cross-linked with cystamine hydrochloride (1 mg mL^{-1}, pH = 5.8, 0.01 M phosphate) for 20 h after activation with carbodiimide solution (5 mg mL^{-1}, pH = 5, 0.01 M phosphate) for 40 min. PVPON was released from the resultant $PMAA_{CS}$ hydrogels during their exposure to pH = 8 for 24 h. The hydrogel particles were further treated in ethylenediaminetetraaceticacid disodium salt (EDTA, 0.1 M) solution at pH = 7 for 3 h followed by dialysis in DI water for 3 d. DOX-loaded $PMAA_{CS}$ hydrogel particles were obtained by incubating the particles with 0.2 mg mL^{-1} DOX solution (pH = 6.4, 0.01 M phosphate) for 24 h followed by rinsing with 0.01 M phosphate solutions at pH = 7.4 five times. The amount of DOX loaded in hydrogel particles was determined by using a DOX calibration curve. The drug loading capacity (DLC, the amount of DOX per particle) was calculated as follows: DLC = (([DOX]i − [DOX]s)/(number of particles)), in which [DOX]i is the initial DOX concentration and [DOX]s is the concentration of DOX in supernatant after particle loading. The number of particles was counted using a hemacytometer (Fisher Scientific).

Scanning Electron Microcopy. The shape and morphology of $PMAA_{CS}$ hydrogel particles were examined by using an FEI Quanta FEG SEM microscope at 10 kV. Samples were prepared by depositing a drop of a particle suspension on a silicon wafer and allowing it to dry overnight at room temperature. Before imaging, dried specimens were sputter-coated with an ∼5 nm thick gold layer using a Denton sputter-coater.

Fourier Transform Infrared Spectroscopy. Infrared spectra of freeze-dried $(PMAA/PVPON)_5$ hydrogen-bonded templates and their cross-linked $(PMAA_{CS})_5$ counterparts were collected with a Bruker Alpha FT-IR spectrometer in transmission mode under ambient conditions.

ζ-Potential Measurements. Surface charge of the (PMAA/PVPON) and $PMAA_{CS}$ particles was obtained by measuring their ζ-potential using a Nano Zetasizer (Malvern). For pH-dependent ζ-potential measurements, the hydrogel particles were collected via centrifugation, and their supernatants were exchanged for 0.01 M phosphate solutions with a certain pH value followed by particle redispersion. In every measurement, a ζ-potential value was obtained by averaging three independent measurements.

Confocal Laser Scanning Microscopy. pH-Response of the nanoporous $(PMAA_{CS})_5$ multilayer hydrogel particles was studied using a Nikon A1R+ confocal laser microscope equipped with a 100× oil immersion objective. A drop of a hydrogel particle suspension was added to a Lab-Tek chambered coverglass filled with buffer solutions at certain pH values; images were taken after the particles settled at the bottom of the chamber.

Turbidity Measurements. Turbidity measurements were performed to trace the GSH-induced degradation of $PMAA_{CS}$ hydrogels at 37 °C using fluorometry (Varian, Cary Eclipse). The scattering intensity of the particle suspension (2×10^5 hydrogels μL^{-1}) at pH = 7.4 in PBS with or without 5 mM GSH was measured at λ = 700 nm. The ratio of the particle scattering intensity at a certain interval to that of the initial nondegraded particles was used to calculate the relative turbidity.

In Vitro Doxorubicin Release. DOX-loaded $(PMAA_{CS})_5$ hydrogel particles (6.7×10^5 hydrogels μL^{-1}) either with or without 5 mM GSH were stirred continuously in PBS solution at pH = 7.4 at 37 °C. At desired time points, the solutions were centrifuged at 8000 rpm for 5 min, and the amount of DOX released from the hydrogels was determined by measuring UV−vis absorbance of supernatants at 490 nm (Varian Cary 50).

Cell Studies. Human cervical carcinoma HeLa cells were used for hydrogel cytotoxicity and cellular internalization studies. For DOX-free $(PMAA_{CS})_5$ hydrogel particle cytotoxicity studies, cells were seeded in wells of a black 96-well glass-bottom plate at a density of 2×10^4 cells per well in Dulbecco's Modification of Eagle's Medium (DMEM; high glucose) supplemented with 10% heat-inactivated fetal bovine serum, and incubated with the $(PMAA_{CS})_5$ hydrogel particles at a particle-to-cell ratio of 100. Incubation was performed at 37 °C in an

DOI: 10.1021/acsami.5b03360
ACS Appl. Mater. Interfaces 2015, 7, 13633−13644

atmosphere of humidity ≥85% and air/CO_2 ratio of 95/5%. Subsequently, at 24, 48, and 72 h intervals, 10 μL of Alamar Blue (Invitrogen) was added directly to cells in culture medium (1/10th volume), and the plates were incubated for another 2 h. Finally, fluorescence was read using a fluorescence excitation/emission λ = 570/585 nm in an Envision reader. Each treatment was analyzed in six replicates. Data were used to calculate cell viability relative to untreated controls.

For cell internalization studies, HeLa cells were plated at a density of 10 000 cells per well in a 96-well plate. Cells were allowed to adhere for 24 h followed by culturing with DOX-free $(PMAA_{CS})_5$, DOX-loaded $(PMAA_{CS})_5$ cubes or spheres, or free DOX solution (0.68 μL, 0.2 mg mL^{-1}) for 1 and 6 h. The particle-to-cell ratio was 20:1. After that, liquid medium was aspirated, and the cells were washed once with PBS and covered to a depth of 2−3 mm with 4% paraformaldehyde diluted in 1X PBS for 20 min. Fixative was aspirated, and cells were rinsed three times with 1X PBS for 5 min each. Subsequently, specimens were blocked for 1 h using 1X PBS, 0.2% Triton X-100, 10% normal serum from the same species as the secondary antibody. Then, a primary antibody against the human early endosome antigen (EEA1 goat antibody, Santa Cruz Biotechnology) was added diluted 1:50 in antibody dilution buffer (1X PBS/1% BSA/0.2% Triton X-100) and incubated overnight at 4 °C under gentle agitation. Cells were rinsed three times with 1X PBS for 5 min each and incubated for 1 h at room temperature in the dark with a fluorophore-conjugated secondary antibody (Donkey anti-Goat IgG secondary antibody Alexa Fluor 488 conjugate, Life Technologies) diluted 1:200 in antibody dilution buffer. Finally, after rinsing three times with 1X PBS, cells were incubated with DAPI to stain the cell nuclei. Fluorescent optical sections were collected with Nikon A1R+ confocal laser microscope system equipped with a 100× oil immersion objective using a TRITC/Alexa488/DAPI filter set. Multiple optical sections were imaged for each microscopic field.

The anticancer potential of DOX-loaded $(PMAA_{CS})_5$ hydrogel particles was studied using HeLa cells. The cells were plated in glass-bottom 96-well black plates at 2×10^4 cells per well. The DOX-loaded cubical or spherical hydrogels were added at 100 particles per cell (four replicates for each condition). Particle-free supernatant of the particle suspension was used as a negative control. The same volume of supernatant as that of DOX-loaded hydrogel suspension was used for each case. The equal amount of DOX (6.8 μL; 0.2 mg mL^{-1}) was used as a positive control of cytotoxicity assessment. The cells were incubated in a humidified atmosphere at 37 °C with 5% CO_2 for 3, 10, 24, and 48 h. After each time point, 10 μL of Alamar Blue (Invitrogen) was added directly to cells in culture medium (1/10th volume), and the plates were incubated for another 2 h. Subsequently, fluorescence was read using a fluorescence excitation/emission λ = 570/585 nm in an Envision reader. Data were presented as a mean ± standard deviation and analyzed using a two-tailed *t*-test. The level of significant difference between mean values for each experimental group was set at a probability of $p < 0.05$.

RESULTS AND DISCUSSION

Cystamine-Cross-Linked $(PMAA_{CS})_n$ Hydrogel Films: Fabrication, pH-Response, and Biodegradation. CS-cross-linked PMAA hydrogels were first prepared and characterized on flat templates. PMAA was assembled with PVPON into nanothin hydrogen-bonded planar multilayers from 0.5 mg mL^{-1} polymer solutions at pH = 2.5 as shown in Scheme 1 (1). The PMAA layers within the (PMAA/PVPON) hydrogen-bonded multilayer template were then cross-linked with CS, and PVPON was released from the $(PMAA_{CS})_n$ hydrogel multilayer at pH = 8 (0.01 M phosphate) (Scheme 1; 2−3). Since the CS molecule has a disulfide group and two additional methylene groups in its chemical structure as compared to EDA, there existed a concern that a more hydrophobic CS linker could adversely affect the pH-responsive behavior of the multilayer hydrogel or shift the pH-dependent swelling regions to extremely basic and acidic conditions. Figure 1a shows that multilayer hydrogels of $(PMAA_{CS})_5$ and

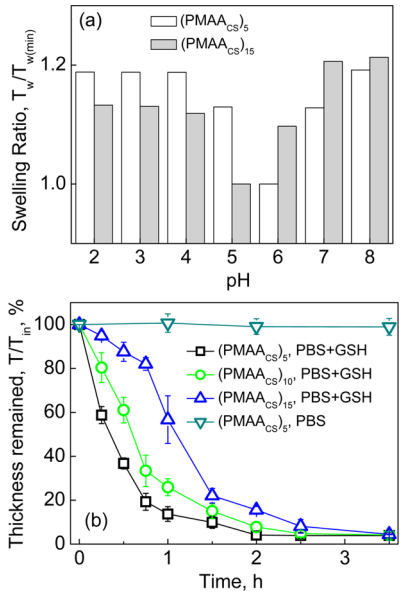

Figure 1. (a) pH-dependent $(PMAA)_5$ and $(PMAA)_{15}$ hydrogel film swelling ratios, $T_w/T_{w(min)}$ (the ratio between wet film thickness at a certain pH, T_w and the minimal wet thickness of the film, $T_{w(min)}$) as measured by in situ ellipsometry. (b) Degradation of CS-cross-linked $(PMAA_{CS})_n$ multilayer hydrogel films (n = 5; 10; 15 layers) in the presence of 5 mM GSH in PBS (pH = 7.4, 37 °C) as the percentage of thickness remained after the treatment calculated as the ratio of $PMAA_{CS}$ hydrogel thickness at a certain time point T to the initial hydrogel thickness T_{in}.

$(PMAA_{CS})_{15}$ with corresponding dry thicknesses of 26 and 67 nm demonstrated pH-dependent swelling at pH > 6 and pH < 5 due to mutual repulsion of the ionized carboxylic and amino groups, respectively, similar to that observed for PMAA multilayer hydrogels cross-linked with EDA as measured by in situ ellipsometry.[48,49] However, we observed a shift in the pH value at which the minimum hydrogel swelling is observed for thicker hydrogels from pH = 6 for $(PMAA_{CS})_5$ to pH = 5 for $(PMAA_{CS})_{15}$ (Figure 1a and Supporting Information, Figure S1). This change can be attributed to a more hydrophobic microenvironment within $(PMAA_{CS})_5$ unlike that of $(PMAA_{CS})_{15}$ because of a higher $(PMAA_{CS})_5$ cross-link density compared to that of $(PMAA_{CS})_{15}$. The average cross-link densities of the hydrogels were 71 and 122 monomer units between two cross-links for $(PMAA_{CS})_5$ and $(PMAA_{CS})_{15}$, respectively, as calculated from nonionic swelling (at minimum multilayer hydrogel swelling) measured by in situ ellipsometry using the Flory equation for one-dimensional swelling of nonionic gels.[49] The hydration ratio of $(PMAA_{CS})_5$ was calculated as the ratio of the difference between the wet film thickness at the minimum film swelling T_w and its dry thickness T_d, and the film's dry thickness. This ratio $(T_w - T_d)/T_d$ was 45% lower than that for $(PMAA_{CS})_{15}$, yielding 2.2- and 3.2-fold, respectively. A similar shift of the hydrogel swelling response toward a higher pH value was observed for EDA-cross-linked poly(2-ethylacrylic acid) (PEAA) hydrogels, where higher charge densities were needed to expand the PEAA multilayer hydrogel compared to that of the less hydrophobic PMAA.[50] The more hydrophobic nature of CS-cross-linked PMAA hydrogels is also evident from the smaller overall swelling

DOI: 10.1021/acsami.5b03360
ACS Appl. Mater. Interfaces 2015, 7, 13633−13644

ratios at pH > 7 observed for $(PMAA_{CS})_5$ and $(PMAA_{CS})_{15}$ compared to that of EDA-cross-linked PMAA systems. Both were prepared by dipping under similar conditions with the corresponding maximum swelling ratios of 1.2 for $PMAA_{CS}$ versus 2.5 for $PMAA_{EDA}$.[49]

Since disulfide bonds in the CS cross-links of $PMAA_{CS}$ hydrogels can be reduced to thiols in the presence of intracellular GSH concentration of 5 mM, we studied the biodegradation of CS-cross-linked PMAA hydrogel films in the presence of GSH using ellipsometry. The dry thickness of the planar $(PMAA_{CS})_5$, $(PMAA_{CS})_{10}$, and $(PMAA_{CS})_{15}$ hydrogels exposed to 5 mM GSH solution in PBS (pH = 7.4) at 37 °C was measured at certain time intervals. As a negative control, $(PMAA_{CS})_5$ films exposed to the PBS solution without GSH under the same conditions was used. The extent of degradation of each planar hydrogel was characterized by the percentage of thickness remaining after the treatment; calculated as the ratio of hydrogel thickness at a certain time point T to the initial hydrogel thickness T_{in}. Figure 1b demonstrates that no loss of thickness was observed for $(PMAA_{CS})_5$ hydrogels without GSH treatment, while the ratio of thickness for $(PMAA_{CS})_5$, $(PMAA_{CS})_{10}$, and $(PMAA_{CS})_{15}$ decreased to 37 ± 3, 61 ± 6 and 86 ± 4%, respectively, after 30 min of the GSH treatment. The complete degradation of the $(PMAA_{CS})_5$, $(PMAA_{CS})_{10}$, and $(PMAA_{CS})_{15}$ hydrogels (due to reduction of the disulfide links to thiol groups and subsequent hydrogel disassembly) was observed after 2, 2.5, and 3.5 h of the treatment, respectively (Figure 1b). The slightly longer times required for dissolution of $(PMAA_{CS})_{10}$ and $(PMAA_{CS})_{15}$ hydrogels compared to $(PMAA_{CS})_5$ are explained by their larger initial thicknesses (44 and 67 nm vs 26 nm, respectively).

$PMAA_{CS}$ Hydrogel Particles: Fabrication and Properties. To obtain the degradable $PMAA_{CS}$ hydrogel particles, 2 μm porous Mn_2O_3 cubic and spherical cores were used as sacrificial templates.[16] As Figure 2a schematically shows, hydrogen-bonded (H-bonded) complexes of PMAA/PVPON were formed LBL inside PEI-coated porous Mn_2O_3 particles using five deposition cycles at pH = 3.5 (0.01 M phosphate), followed by dissolution of the inorganic template by exposing the $(PMAA/PVPON)_5$-modified particles to 1 M HCl solution for 24 h. After the H-bonded multilayer 3D particles were thoroughly rinsed with aqueous pH = 2 solution (Figure 2a(3)), PMAA layers were CS-cross-linked for 20 h, and PVPON was released from the $(PMAA_{CS})_5$ hydrogel particles during their exposure to pH = 8 for 24 h (Figure 2a(4)).

The Fourier transform infrared (FT-IR) spectrum of the freeze-dried $(PMAA/PVPON)_5$ H-bonded particles shows the absorption band at 1694 cm^{-1} characteristic of stretching vibrations of the protonated carboxylic groups of PMAA, whereas the absorption band at 1650 cm^{-1} is attributed to the carbonyl stretching vibrations in PVPON[37] (Supporting Information, Figure S2). The release of PVPON from $(PMAA_{CS})_5$ hydrogel particles after cross-linking was confirmed by the disappearance of the absorption band at 1650 cm^{-1} in the FT-IR spectrum of the hydrogel particles freeze-dried from solution at pH = 8. The new absorption band at 1617 cm^{-1} for $(PMAA_{CS})_5$ particles freeze-dried from solution at pH = 3.5 corresponds to amide I peak and indicates the linkages between amine and carboxyl groups in CS and PMAA, respectively (Figure S2). The shift from 1541 cm^{-1} corresponding to ionized $-COO^-$ groups to 1649 cm^{-1} corresponding to protonated $-COOH$ groups in the spectra for particles freeze-dried from pH = 8 and pH = 3.5,[37,48] respectively, confirms the presence of functional pH-responsive carboxylic groups in the hydrogel particles of $(PMAA_{CS})_5$.

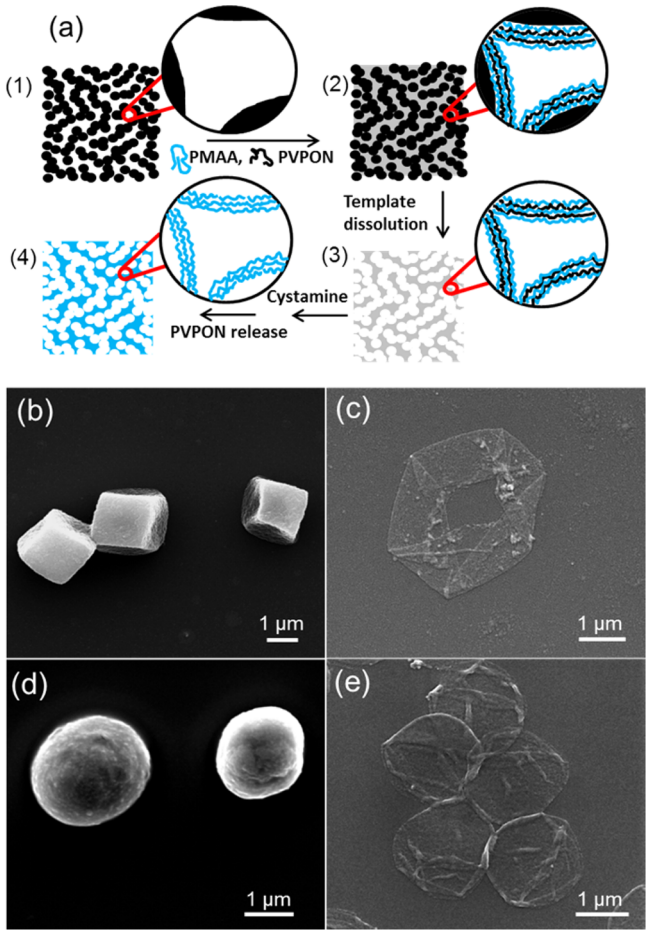

Figure 2. (a) Synthesis of nanoporous hydrogel particles made of CS-cross-linked $PMAA_{CS}$ multilayers: Inside PEI-coated porous Mn_2O_3 cubic or spherical particles (1) hydrogen-bonded complexes of PMAA/PVPON are formed LBL (2). After dissolution of the inorganic template (3), PMAA layers are cross-linked with CS and PVPON is released from $PMAA_{CS}$ multilayer hydrogel particle (4). SEM images of (b, c) cubic and (d, e) spherical $(PMAA_{CS})_5$ multilayer hydrogel (b, d) particles and (c, e) capsules.

Scanning electron microscopy (SEM) images of the $(PMAA_{CS})_5$ hydrogels prepared using spherical and cubical manganese oxide templates revealed that they retained their respective 3D shapes in the dry state (Figure 2b,d), while the corresponding $(PMAA_{CS})_5$ hydrogel capsules prepared on nonporous manganese carbonate templates, although replicating the shape of the templates in solution, collapsed upon drying (Figure 2c,e). The ability of the multilayer hydrogel particles to preserve their 3D structure indicates that both PMAA and PVPON polymers can infiltrate into the pores of Mn_2O_3 during the deposition process and that the (PMAA/PVPON) multilayers are formed inside pores, a result similar to previously reported poly(acrylic acid)/poly(allylamine hydrochloride) (PAA/PAH) ionically paired multilayers.[51]

The pH-controlled reversal of surface charge for $(PMAA_{CS})_5$ hydrogel particles was observed using ζ-potential measurements of the particle suspensions in 0.01 M phosphate solutions prepared at certain pH values. Figure 3a demonstrates that before cross-linking, the ζ-potential was negative for cubical and spherical $(PMAA/PVPON)_5$ particles (with values

DOI: 10.1021/acsami.5b03360
ACS Appl. Mater. Interfaces 2015, 7, 13633−13644

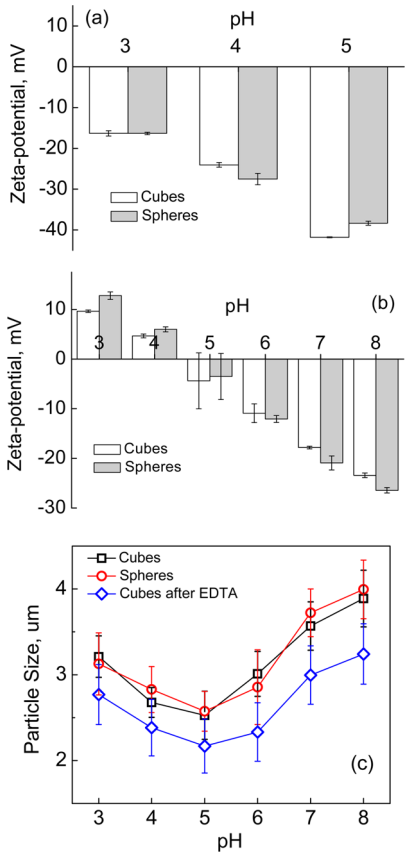

Figure 3. (a) pH-Dependent variations of ζ-potential for hydrogen-bonded $(PMAA/PVPON)_5$ template-free particles. (b) pH-Dependent variations of ζ-potential values for cubic and spherical template-free $(PMAA_{CS})_5$ hydrogel particles. (c) pH-Dependent size variations of cubic and spherical $(PMAA_{CS})_5$ hydrogel before (□, ○) and after EDTA treatment (◇).

of −16.3 ± 0.7 and −41.8 ± 0.1 mV for cubic and −16.3 ± 0.3 and −38.4 ± 0.5 mV for spherical at pH = 3 and pH = 5, respectively). The negative surface charge of the H-bonded template particles is because of the carboxyl groups within the PMAA segments not involved in H-bonding with PVPON.[32] After cross-linking with CS and release of PVPON from the multilayer hydrogel networks, the surface charge of $(PMAA_{CS})_5$ at pH = 3 became slightly positive, yielding the ζ-potential values of 9.6 ± 0.3 and 13 ± 1 mV for the hydrogel cubes and spheres, respectively (Figure 3b). Also, in contrast to the H-bonded templates, the surface charge of the hydrogel particles was neutral at pH = 5 with the ζ-potential values oscillating around 0 mV (Figure 3b). The positive surface charge of the $(PMAA_{CS})_5$ hydrogel particles at pH < 5 is because of the protonation of free amine groups in singly attached CS molecules (where only one molecule end participates in cross-linking), while negative ζ-potential values at pH > 5 are due to ionized carboxylates from PMAA (Figure 3b).

The ionization of the available amine or carboxylic groups in the $(PMAA_{CS})_5$ hydrogel particles at pH < 5 or pH > 5, respectively, resulted in pH-controlled reversible changes in the hydrogel particle dimensions as observed using confocal microscopy. For instance, both $(PMAA_{CS})_5$ cubes and spheres increased in size when transferred from pH = 5 to pH = 3 by 1.3 ± 0.1 and 1.2 ± 0.1 fold, and again when transferred from pH = 5 to pH = 8 increased by 1.6 ± 0.1 and 1.5 ± 0.1 fold, respectively. The $(PMAA_{CS})_5$ hydrogel cubes increased from 2.5 ± 0.2 μm to 3.9 ± 0.3 μm when the solution pH was changed from pH = 5 to pH = 8 and to 3.2 ± 0.2 μm at pH = 3 (Figure 3c). Similarly, the $(PMAA_{CS})_5$ spherical hydrogels increased from 2.6 ± 0.2 μm at pH = 5 to 4.0 ± 0.3 μm at pH = 8 and to 3.1 ± 0.4 μm at pH = 3 (Figure 3c). However, despite the change in size, the particles impressively maintained their 3D shape (Supporting Information, Figure S3).

After cubical $(PMAA_{CS})_5$ hydrogel particles were incubated in 0.1 M EDTA solution at pH = 7 for 3 h, the size of the hydrogel particles at pH = 5 slightly decreased from 2.5 ± 0.3 to 2.2 ± 0.3 μm (Figure 3c) implying that some Mn^{2+} ions could be still trapped in the (PMAA/PVPON) templates upon core dissolution and need to be removed from the particles to render them cytocompatible. However, the effect on swelling behavior of lingering manganese ions from the dissolved manganese oxide cores was found negligible. After EDTA purification of $(PMAA_{CS})_5$ hydrogel cubes, the overall swelling at pH = 3 and pH = 8 was 1.3 ± 0.1 and 1.5 ± 0.1-fold, respectively, and did not differ from the hydrogels before purification (Figure 3c). The $(PMAA_{CS})_5$ hydrogel particles showed a swelling profile similar to that of our previously demonstrated nondegradable EDA-linked hydrogel particles.[16] However, the overall swelling ratios (the ratio of the particle size at a certain pH to the minimum size of the hydrogel particle at pH = 5) were smaller than those of the EDA-cross-linked cubes or spheres, which underwent a nearly twofold reversible swell/shrink response to pH variations.[16] The lower 1.5−1.2-fold swelling ratios of the $(PMAA_{CS})_5$ biodegradable hydrogels can be explained by a more hydrophobic nature of those structures because of a more hydrophobic CS linker as discussed above for planar $PMAA_{CS}$ hydrogels.

Shaped $PMAA_{CS}$ Hydrogel Particles: Loading and Release of DOX in Situ. The anticancer drug DOX was loaded inside both spherical and cubical $(PMAA_{CS})_5$ particles of 2 μm by soaking them in 0.2 mg mL^{-1} DOX solution at pH = 6.4 for 24 h followed by rinsing with pH = 7.4 buffer (0.01 M phosphate). Confocal microscopy images of the DOX-loaded $(PMAA_{CS})_5$ hydrogels demonstrate that the drug was homogeneously loaded throughout the particle volume (Figure 4a,b). In contrast, the thiol-modified PMAA hydrogel capsules

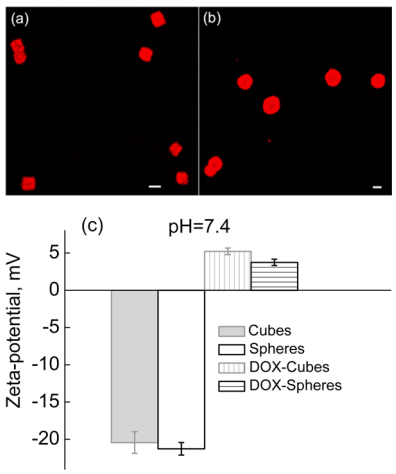

Figure 4. CLSM images of (a) cubic and (b) spherical $(PMAA_{CS})_5$ hydrogel particles loaded with DOX. (c) Comparison of ζ-potential values of DOX-free (gray, white) and DOX-loaded (vertical and horizontal stripes) cubic and spherical $(PMAA_{CS})_5$ hydrogel particles at pH = 7.4 (0.01 M phosphate).

DOI: 10.1021/acsami.5b03360
ACS Appl. Mater. Interfaces 2015, 7, 13633−13644

reported earlier can only load DOX or other small drugs mainly in the hydrogel capsule wall because of ionic and hydrophobic interactions between the drug molecules and the negatively charged PMAA shell and require using lipophilic phases or surfactants to entrap DOX in the capsule interior.[26,52] The difficulty of retaining DOX inside the thiol-modified PMAA capsule cavity results in the leakage of drug molecules from the capsule because of the enhanced permeability of the capsule shell at physiological pH.[52] In the multilayer hydrogel particles studied here, the $PMAA_{CS}$ film is "packed" throughout the volume of the particle, therefore providing an enormous area of interaction for the drug unlike in the hollow hydrogel capsules. Moreover, the accumulation of positive charge within the $PMAA_{CS}$ hydrogel particles at pH < 5 can facilitate their endosomal/lysosomal escape via inducing endosomal disruption because of the hydrogel swelling.[5,53,54]

After DOX-loading, the $(PMAA_{CS})_5$ multilayer hydrogel particles reversed their surface charge from the negative ζ-potential values of -20 ± 1 and -21.3 ± 0.9 mV to the slightly positive 5.2 ± 0.5 and 3.8 ± 0.4 mV for the cubes and spheres, respectively, as observed from the ζ-potential measurements of the hydrogels at pH = 7.4 (0.01 M phosphate; Figure 4c). This positive surface charge can be attributed to the presence of positively charged DOX molecules ($pK_a = 8.3$) at the hydrogel particle surfaces. The positive charge of the DOX-loaded $(PMAA_{CS})_5$ hydrogel particles can facilitate their uptake by cells because of their interactions with negatively charged cell membranes.[55,56] The DOX loading capacity of the cubical and spherical hydrogels was found to be $(6.8 \pm 0.2) \times 10^{-4}$ and $(6.2 \pm 0.8) \times 10^{-4}$ ng per particle, respectively.

The degradation of the $(PMAA_{CS})_5$ hydrogel microparticles in the presence of intracellular concentrations of GSH was evaluated using turbidity measurements.[47] The relative turbidity, defined as the ratio of the $(PMAA_{CS})_5$ hydrogel particle solution scattering intensity at certain time points to the initial scattering intensity, was measured in the presence of 5 mM GSH solution in PBS (pH = 7.4, 37 °C) using fluorescence spectrophotometry. With no GSH in the hydrogel suspension, the relative turbidity of $(PMAA_{CS})_5$ hydrogels did not change with time indicating chemical stability of the hydrogel particles (Figure 5a). GSH treatment provided complete hydrogel particle degradation in 3 h, which is in agreement with the planar hydrogel data discussed above (Figure 5a).

The slightly faster degradation of hydrogel spheres compared to cubes observed within the first hour (with the relative turbidites of 40 ± 3 and 50 ± 2%, respectively) can be explained by a 1.9-fold larger hydrogel cube volume compared to that of the sphere of the same size, that is, when the length of a cube side is the diameter of a spherical particle. The reduction of the disulfide groups within $PMAA_{CS}$ multilayer hydrogels to corresponding thiols in the cytoplasm should result in release of initial polymer chains with M_w of 21 kDa with an average radius of gyration R_g = 1.8 nm (assuming the PMAA persistence length of 0.3 nm),[57] which should ensure a rapid renal clearance of the degraded polymer matrix (renal retention threshold is 30 kDa).[56,58,59]

The release of DOX from DOX-loaded degradable $(PMAA_{CS})_5$ hydrogel cubes and spheres in the presence of 5 mM GSH (PBS, pH = 7.4, 37 °C) was quantified using UV–vis spectroscopy. We found that after 1 h, the amount of DOX released under conditions of the typical intracellular microenvironment was 46 ± 5 and 44 ± 4% from cubical and spherical $(PMAA_{CS})_5$ hydrogels, respectively, (Figure 5b) and saturated at 87 ± 3 and 86 ± 3% for the cubes and spheres, respectively, after 10 h. In the absence of GSH, the cumulative release of DOX from the $(PMAA_{CS})_5$ cubical hydrogels was only 14 ± 3% after their 22 h of incubation in PBS solution at pH = 7.4 and 37 °C (Figure 5b).

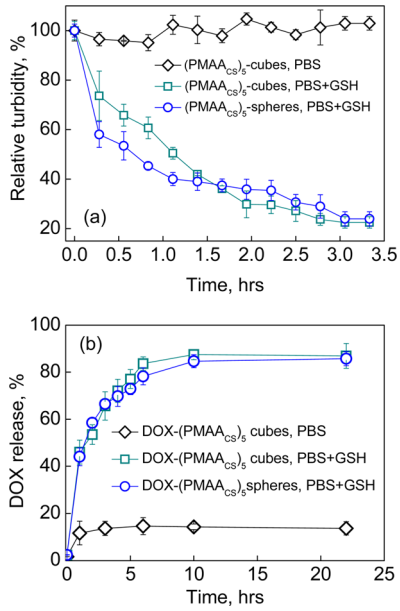

Figure 5. (a) Degradation of CS-cross-linked $(PMAA_{CS})_5$ hydrogel particles in the presence of 5 mM GSH at pH = 7.4 (PBS, 37 °C) as monitored via relative turbidity measurements performed using fluorometry (λ = 700 nm). (b) Release of DOX from cubic and spherical DOX-loaded $(PMAA_{CS})_5$ hydrogels in the presence of 5 mM GSH in PBS buffer (pH = 7.4) at 37 °C as monitored by UV–vis spectroscopy.

Shaped $PMAA_{CS}$ Hydrogel Particles: Release of DOX in Vitro. Interactions of spherical and cubical DOX-loaded $(PMAA_{CS})_5$ degradable hydrogels with human cervical carcinoma cells (HeLa) were explored. The results were compared with the internalization of the corresponding DOX-free hydrogel particles as well as with free DOX solution. Figure 6 demonstrates the representative confocal microscopy images of HeLa cells incubated for 1 h with DOX-free $(PMAA_{CS})_5$ hydrogel cubes and spheres (Figure 6a,b, respectively), free DOX solution (Figure 6c), and DOX-loaded $(PMAA_{CS})_5$ cubes and spheres (Figure 6d,e, respectively). HeLa cell nuclei and cytoplasm endosomes/lysosomes appear in blue (DAPI signal) and green (Alexa Fluor 488 signal), respectively. The bright red fluorescence from DOX within HeLa cell nuclei indicates effective drug transport into the cancer cell nuclei. Though the red DOX fluorescence is colocalized with the blue fluorescence signal from the cell nuclei, there is no signal of DOX in the cytoplasm, which appears green because of Alexa Fluor 488-labeled endosomes/lysosomes (Figure 6). Delivery of DOX into cells by nonstimuli-responsive drug carriers has a low efficiency as the drug is usually trapped with delivery vehicles in the endosomes/lysosomes.[60] Our results suggest a fast internalization of $(PMAA_{CS})_5$ hydrogels and a fast escape of particle-loaded DOX from lysosomes to enter to the cell nuclei.

The slightly positive surface charge of the DOX-loaded hydrogel particles can readily facilitate entry inside cells through an endosomal internalization pathway because of enhanced particle-cell membrane interactions. The lower

DOI: 10.1021/acsami.5b03360
ACS Appl. Mater. Interfaces 2015, 7, 13633–13644

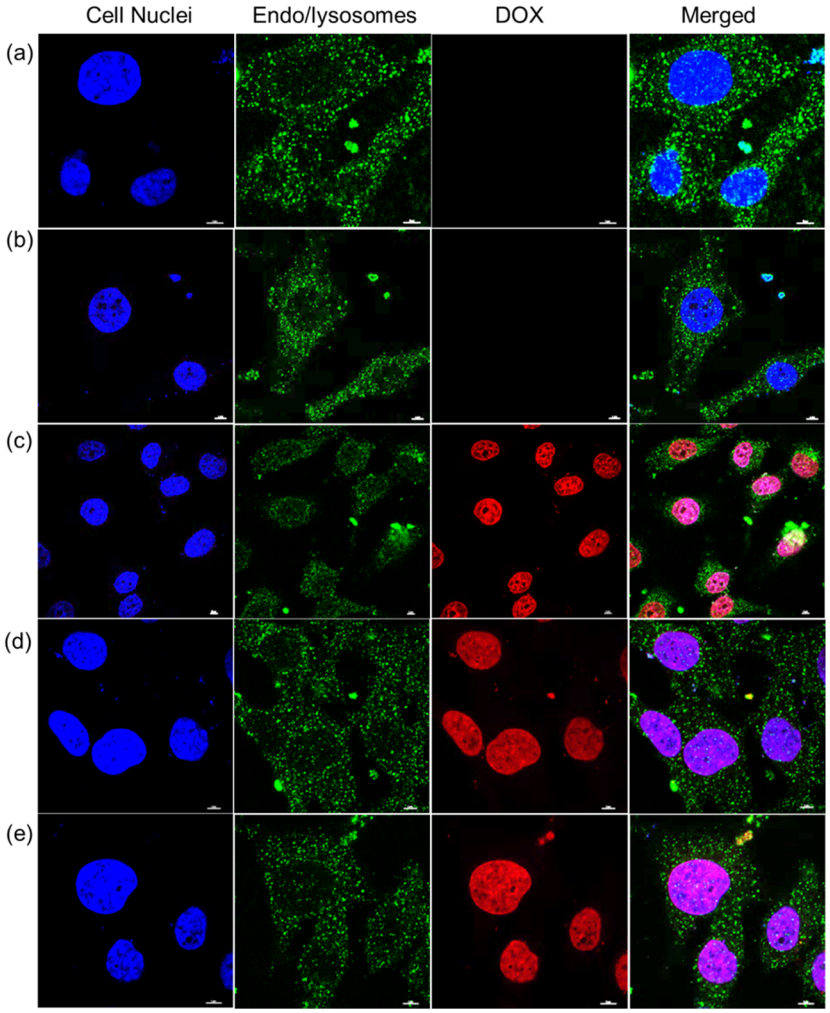

Figure 6. CLSM images of confocal sections of HeLa cells after 1 h of incubation with $(PMAA_{CS})_5$ hydrogel (a) cubes and (b) spheres, and with (c) DOX and DOX-loaded $(PMAACS)_5$ (d) cubes and (e) spheres. The cell nuclei and lyso/endosomes were stained with DAPI (blue) and Alexa Fluor 488-conjugated antibody (green), respectively, while DOX emits a red fluorescence signal. Scale bar is 5 μm in all images.

endosomal/lysosomal pH (pH = 6.5−5 in endosomes and pH = 4 in primary/secondary lysosomes) and the presence of reducing agents (e.g., γ-interferon-inducible lysosomal thiol reductase) may cause a lower pH-triggered increase of $(PMAA_{CS})_5$ particle volume and its partial degradation resulting in endosomal/lysosomal vesicle rapture and DOX release into the cytosolic space.[61] Finally, the disulfide bonds of the $PMAA_{CS}$ hydrogel will be further reduced by intracellular GSH causing dissolution of the $PMAA_{CS}$ matrix into small molecular weight polymer chains as discussed above. Indeed, confocal microscopy images of HeLa cells incubated with the cubical (Figure 7a,b) and spherical (Figure 7c,d) hydrogel particles for 6 h revealed that the particles (indicated by arrows) internalized by the cells significantly decreased in size. The particle shape became impossible to distinguish by confocal microscopy after 6 h of incubation with the cells because of the particle degradation.

To evaluate the therapeutic properties of the degradable multilayer hydrogel cubes and spheres, HeLa cells were incubated with DOX-free or DOX-loaded $(PMAA_{CS})_5$ hydrogel particles at a particle-to-cell ratio of 100:1 for 48 h, and their cytotoxicity to the cells was measured after certain time intervals.

The viability of the cells incubated with the DOX-free $(PMAA_{CS})_5$ hydrogels did not decrease after 24, 48, or 72 h and stayed above 97% even after 72 h of incubation as determined by Alamar Blue cell viability assay (Figure 8a) indicating that without DOX the hydrogel particles are nontoxic to the cancer cells. This agrees with previous reports on PMAA-based micro/nanogels[16,23,54] and hydrogel capsules[36,59] where cross-linker type and synthesis method did not affect the cytocompatibility of the delivery systems.

In contrast, when DOX-loaded $(PMAA_{CS})_5$ hydrogel particles were incubated with the cells, the cell viability decreased gradually within 24 h of incubation (Figure 8b). Free DOX solution with the concentration matching that in the hydrogel particle aliquots was used as a positive control for cell cytotoxicity. After 10 h of incubation, the cell viability decreased from 92 ± 1 to 87 ± 2% and from 90 ± 2 to 75 ± 4% for cubical and spherical hydrogels, respectively, implying the effect of particle shape on the hydrogel particle internalization during the first few hours of cell incubation (Figure 8b). However, after 24 h of the exposure, both cubical and spherical DOX-loaded $(PMAA_{CS})_5$ hydrogel particles were equally cytotoxic to the cancer cells killing almost half of the cells. After another 24 h of incubation the DOX-loaded hydrogel cell cytotoxicity reached almost 90% (Figure 8c).

DOI: 10.1021/acsami.5b03360
ACS Appl. Mater. Interfaces 2015, 7, 13633−13644

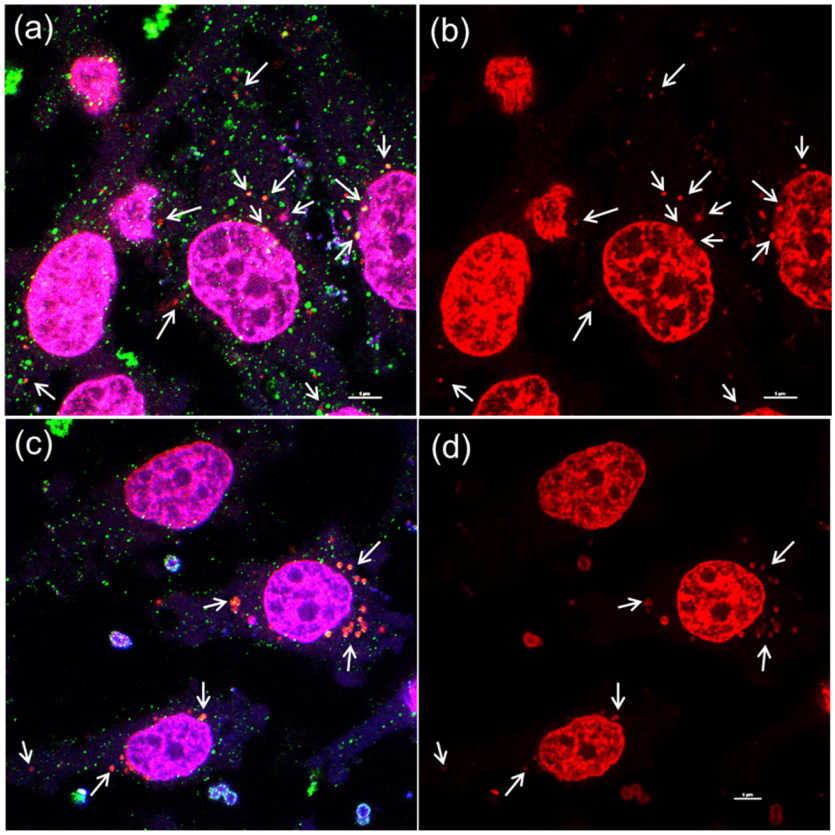

Figure 7. Confocal microscopy images of HeLa cells after 6 h of incubation with DOX-loaded $(PMAA_{CS})_5$ multilayer hydrogel (a, b) cubes and (c, d) spheres. The images show superimposed confocal sections of DAPI-stained nuclei (blue channel), Lyso tracker-stained lysosomes/endosomes in the cytosol (green channel, Alexa Fluor 488-conjugated antibody fluorescence), and DOX (red channel). The only red channel confocal sections (b, d) demonstrate presence of DOX inside cell nuclei as well as remaining parts of DOX-loaded hydrogel particles in the cell plasma. The arrows point to remaining internalized hydrogel particles, which are colocalized with intracellular endo/lysosomes in the cell cytosol. Scale bar is 5 μm.

Our results on cell internalization (Figures 6 and 7) and cell viability in the presence of the DOX-loaded cubical and spherical hydrogels (Figure 8b,c) indicate that once the particles were taken up by cells, DOX was rapidly released to enter the cell nuclei and kill the cells. Since the amounts of DOX loaded in the cubical and spherical hydrogels were similar (6.8×10^{-4} ng and 6.2×10^{-4} ng per particle, respectively), the 12% higher cell cytotoxicity observed for the $(PMAA_{CS})_5$ hydrogel spheres as compared to that of the cubes within the first 10 h of incubation reflect the effect of the hydrogel particle shape on cellular internalization.

Cellular internalization of particles with different shapes can occur either by penetration[62] or wrapping,[63] which involve various pathways.[64] Recent simulations of membrane wrapping around spherical and cubical particles[65] demonstrated that the particle adhesion to the cell and complete cell membrane wrapping around it are controlled by the competition between the adhesion energy gain for particle-cell membrane contact and the energy cost for the lipid bilayer deformation. The adhesion strength for a cube should be threefold more than that of a sphere to compensate the membrane deformation energy at the upper edges of the cube.[65] Because of a higher wrapping energy barrier for cubes compared to that for spheres, spheres can be internalized faster than cubes. Indeed, our results on 12% higher cell cytotoxicity observed for the $(PMAA_{CS})_5$ hydrogel spheres as compared to that of the cubes within the first 10 h of incubation agree well with those simulation results and indicate that the membrane adhesion process plays a more important role in the initial steps of cell internalization for the hydrogel cubes. However, since eventually both DOX-loaded $(PMAA_{CS})_5$ spheres and cubes demonstrated similar cytotoxicity after longer incubation times of 24 and 48 h, and given their similar DOX payload, long-term amounts of the hydrogel cubes or spheres internalized by HeLa cancer cells seem to be similar.

CONCLUSIONS

We demonstrated intracellular degradable pH-responsive cubic PMAA hydrogel particles synthesized via the multilayer template approach using sacrificial mesoporous manganese oxide particles as templates. The disulfide-containing PMAA hydrogel cubes can increase in size at neutral (pH > 6) and slightly acidic (pH < 6) conditions with the former pH-induced swelling facilitating drug loading within the network, while the latter provides the escape of the DOX-loaded hydrogels from endosomes/lysosomes and release of the drug into the cytosolic space. The degradation of the particles rapidly occurs upon exposure to the intracellular concentration of GSH (5 mM) within 3 h resulting in the release of small molecular weight polymer chains (21 kDa), which should ensure a rapid renal clearance of the degraded polymer matrix in vivo. The PMAA cubes and spheres were demonstrated to be noncytotoxic to HeLa cancer cells; however, DOX-loaded PMAA hydrogel particles demonstrated 50% and 90% cytotoxicity to the cells when incubated with the cells for 24 and 48 h, respectively. Finally, we observed the effect of the particle shape on the cell

DOI: 10.1021/acsami.5b03360
ACS Appl. Mater. Interfaces 2015, 7, 13633−13644

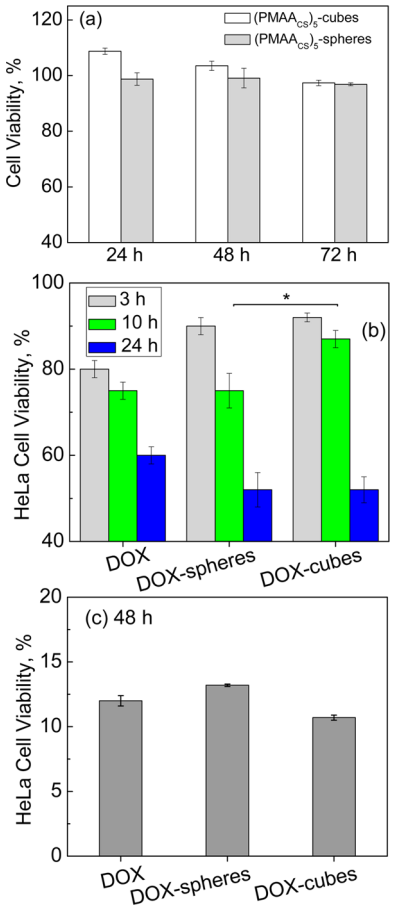

Figure 8. (a) Viability of HeLa cells (%) after incubation with $(PMAA_{CS})_5$ hydrogel particles for 24, 48, and 72 h (particle-to-cell ratio is 100:1). Viability of HeLa cell (% of negative control) after (b) 3, 10, 24 and (c) 48 h of incubation with free DOX, and DOX-loaded $(PMAA_{CS})_5$ cubes and spheres. Particle-free supernatants from suspensions of the DOX-loaded cubes and spheres were used as a negative control with the same volume as that of DOX-loaded particle suspensions. Each data point represents an average of four replicates ± standard deviation (* $p < 0.05$).

internalization within the first 10 h of cell incubation. The DOX-loaded $(PMAA_{CS})_5$ spheres exhibited 12% higher cell cytotoxicity when incubated with the HeLa cells for 10 h as compared to that of the $(PMAA_{CS})_5$ cubes. The latter indicated a more important role of the membrane adhesion process in the initial steps of cell internalization for the hydrogel cubes. We believe that the presented approach integrates the advantages of shape and pH-sensitivity for novel types of "intelligent" 3D networks with programmable shape-regulating behavior for use in controlled delivery of therapeutics.

■ ASSOCIATED CONTENT

Supporting Information

Ellipsometry data for pH-dependent thicknesses of the (PMAA/PVPON) hydrogen-bonded and degradable (PMAA) multilayer hydrogel planar films, optical microscopy images of cubic and spherical multilayer hydrogel particles, and FT-IR data for degradable multilayer hydrogels at pH = 8 and pH = 3.5. The Supporting Information is available free of charge on the ACS Publications website at DOI: 10.1021/acsami.5b03360.

■ AUTHOR INFORMATION

Corresponding Author

*E-mail: ekharlam@uab.edu.

Author Contributions

⊥The authors equally contributed to this work

Notes

The authors declare no competing financial interest.

■ ACKNOWLEDGMENTS

This work was supported by NSF Career Award No. 1350370. We thank Mr. A. Alford of the Univ. of Alabama at Birmingham (UAB) for technical assistance. The UAB SEM and High Resolution Imaging facility is also acknowledged.

■ REFERENCES

(1) Zhang, Y.; Chan, H. F.; Leong, K. W. Advanced Materials and Processing for Drug Delivery: The Past and the Future. *Adv. Drug Delivery Rev.* **2013**, *65*, 104−120.

(2) Venkataraman, S.; Hedrick, J. L.; Ong, Z. Y.; Yang, C.; Ee, P. L. R.; Hammond, P. T.; Yang, Y. Y. The Effects of Polymeric Nanostructure Shape on Drug Delivery. *Adv. Drug Delivery Rev.* **2011**, *63*, 1228−1246.

(3) Cohen, K.; Emmanuel, R.; Kisin-Finfer, E.; Shabat, D.; Peer, D. Modulation of Drug Resistance in Ovarian Adenocarcinoma Using Chemotherapy Entrapped in Hyaluronan-Grafted Nanoparticle Clusters. *ACS Nano* **2014**, *8*, 2183−2195.

(4) Yan, Y.; Ochs, C. J.; Such, G. K.; Heath, J. K.; Nice, E. C.; Caruso, F. Bypassing Multidrug Resistance in Cancer Cells with Biodegradable Polymer Capsules. *Adv. Mater.* **2010**, *22*, 5398−5403.

(5) Nel, A. E.; Madler, L.; Velegol, D.; Xia, T.; Hoek, E. M. V.; Somasundaran, P.; Klaessig, F.; Castranova, V.; Thompson, M. Understanding Biophysicochemical Interactions at the Nano-Biointerface. *Nat. Mater.* **2009**, *8*, 543−557.

(6) Cheng, Y.; Zhao, L.; Li, Y.; Xu, Y. Design of Biocompatible Dendrimers for Cancer Diagnosis and Therapy: Current Status and Future Perspectives. *Chem. Soc. Rev.* **2011**, *40*, 2673−2703.

(7) Jin, H.; Huang, W.; Zhu, X.; Zhou, Y.; Yan, D. Biocompatible or Biodegradable Hyperbranched Polymers: From Self-assembly to Cytomimetic Applications. *Chem. Soc. Rev.* **2012**, *41*, 5986−5997.

(8) Rao, J. P.; Geckeler, K. E. Polymer Nanoparticles: Preparation Techniques and Size-Control Parameters. *Prog. Polym. Sci.* **2011**, *36*, 887−913.

(9) Kamaly, N.; Xiao, Z.; Valencia, P. M.; Radovic-Moreno, A. F.; Farokhzad, O. C. Targeted Polymeric Therapeutic Nanoparticles: Design, Development and Clinical Translation. *Chem. Soc. Rev.* **2012**, *41*, 2971−3010.

(10) Yan, Y.; Bjornmalm, M.; Caruso, F. Assembly of Layer-by-Layer Particles and Their Interactions with Biological Systems. *Chem. Mater.* **2014**, *26*, 452−460.

(11) Lv, L. P.; Landfester, K.; Crespy, D. Stimuli-Selective Delivery of Two Payloads from Dual Responsive Nanocontainers. *Chem. Mater.* **2014**, *26*, 3351−3353.

(12) Huang, X.; Appelhans, D.; Formanek, P.; Simon, F.; Voit, B. Tailored Synthesis of Intelligent Polymer Nanocapsules: An Investigation of Controlled Permeability and pH-Dependent Degradability. *ACS Nano* **2012**, *6*, 9718−9726.

(13) Dai, J.; Lin, S. D.; Cheng, D.; Zou, S. Y.; Shuai, X. T. Interlayer-Cross-Linked Micelle with Partially Hydrated Core Showing Reduction and pH Dual Sensitivity for Pinpointed Intracellular Drug Release. *Angew. Chem., Int. Ed.* **2011**, *50*, 9404−9408.

(14) White, E. M.; Yatvin, J.; Grubbs, J. B.; Bilbrey, J. A.; Locklin, J. Advances in Smart Materials: Stimuli-Responsive Hydrogel Thin Films. *J. Polym. Sci., Part B: Polym. Phys.* **2013**, *51*, 1084−1099.

(15) Tokarev, I.; Minko, S. Stimuli-Responsive Porous Hydrogels at Interfaces for Molecular Filtration, Separation, Controlled Release, and Gating in Capsules and Membranes. *Adv. Mater.* **2010**, *22*, 3346−3462.

DOI: 10.1021/acsami.5b03360
ACS Appl. Mater. Interfaces 2015, 7, 13633−13644

(16) Kozlovskaya, V.; Chen, J.; Tedjo, C.; Liang, X.; Campos-Gomez, J.; Oh, J.; Saeed, M.; Lungu, C. T.; Kharlampieva, E. pH-Responsive Hydrogel Cubes for Release of Doxorubicin in Cancer Cells. *J. Mater. Chem. B* **2014**, *2*, 2494−2507.
(17) Beebe, D. J.; Moore, J. S.; Bauer, J. M.; Yu, Q.; Liu, R. H.; Devadoss, C.; Jo, B. H. Functional Hydrogel Structures for Autonomous Flow Control Inside Microfluidic Channels. *Nature* **2000**, *404*, 588−590.
(18) Jiang, Y.; Chen, J.; Deng, C.; Suuronen, E. J.; Zhong, Z. Click Hydrogels, Microgels and Nanogels: Emerging Platforms for Drug Delivery and Tissue Engineering. *Biomaterials* **2014**, *35*, 4969−4985.
(19) Shimoni, O.; Postma, A.; Yan, Y.; Scott, A. M.; Heath, J. K.; Nice, E. C.; Zelikin, A. N.; Caruso, F. Macromolecule Functionalization of Disulfide-Bonded Polymer Hydrogel Capsules and Cancer Cell Targeting. *ACS Nano* **2012**, *6*, 1463−1472.
(20) Cheng, R.; Feng, F.; Meng, F. H.; Deng, C.; Feijen, J.; Zhong, Z. Y. Glutathione-Responsive Nano-Vehicles as a Promising Platform for Targeted Intracellular Drug and Gene Delivery. *J. Controlled Release* **2011**, *152*, 2−12.
(21) Arunachalam, B.; Phan, U. T.; Geuze, H. J.; Cresswell, P. Enzymatic Reduction of Disulfide Bonds in Lysosomes: Characterization of a Gamma-Interferon-Inducible Lysosomal Thiol Reductase (GILT). *Proc. Natl. Acad. Sci. U. S. A.* **2000**, *97*, 745−750.
(22) Chen, W.; Zou, Y.; Meng, F. H.; Cheng, R.; Deng, C.; Feijen, J.; Zhong, Z. Y. Functional Poly(ε-caprolactone)s via Copolymerization of ε-Caprolactone and Pyridyl Disulfide-Containing Cyclic Carbonate: Controlled Synthesis and Facile Access to Reduction-Sensitive Biodegradable Graft Copolymer Micelles. *Macromolecules* **2013**, *46*, 699−707.
(23) Pan, Y. J.; Chen, Y. Y.; Wang, D. R.; Wei, C.; Guo, J.; Lu, D. R.; Chu, C. C.; Wang, C. C. Redox/pH Dual Stimuli-Responsive Biodegradable Nanohydrogels with Varying Responses to Dithiothreitol and Glutathione for Controlled Drug Release. *Biomaterials* **2012**, *33*, 6570−6579.
(24) Chong, S. F.; Sexton, A.; De Rose, R.; Kent, S. J.; Zelikin, A. N.; Caruso, F. A Paradigm for Peptide Vaccine Delivery Using Viral Epitopes Encapsulated in Degradable Polymer Hydrogel Capsules. *Biomaterials* **2009**, *30*, 5178−5186.
(25) Zelikin, A. N.; Li, Q.; Caruso, F. Degradable Polyelectrolyte Capsules Filled with Oligonucleotide Sequences. *Angew. Chem., Int. Ed.* **2006**, *45*, 7743−7745.
(26) Sivakumar, S.; Bansal, V.; Cortez, C.; Chong, S.-F.; Zelikin, A. N.; Caruso, F. Degradable, Surfactant-Free, Monodisperse Polymer-Encapsulated Emulsions as Anticancer Drug Carriers. *Adv. Mater.* **2009**, *21*, 1820−1824.
(27) Champion, J. A.; Mitragotri, S. Shape Induced Inhibition of Phagocytosis of Polymer Particles. *Pharm. Res.* **2009**, *26*, 244−249.
(28) Tao, L.; Hu, W.; Liu, Y.; Huang, G.; Sume, B. D.; Gao, J. Shape-Specific Polymeric Nanomedicine: Emerging Opportunities and Challenges. *Exp. Biol. Med.* **2011**, *236*, 20−29.
(29) Albanese, A.; Tang, P. S.; Chan, W. C. W. The Effect of Nanoparticle Size, Shape, and Surface Chemistry on Biological Systems. *Annu. Rev. Biomed. Eng.* **2012**, *14*, 1−16.
(30) Longmire, M. R.; Ogawa, M.; Choyke, P. L.; Kobayashi, H. Biologically Optimized Nanosized Molecules and Particles: More than Just Size. *Bioconjugate Chem.* **2011**, *22*, 993−1000.
(31) Shah, S.; Liu, Y.; Hu, W.; Gao, J. Modeling Particle Shape-Dependent Dynamics in Nanomedicine. *J. Nanosci. Nanotechnol.* **2011**, *11*, 919−928.
(32) Chen, J.; Kozlovskaya, V.; Goins, A.; Campos-Gomez, J.; Saeed, M.; Kharlampieva, E. Biocompatible Shaped Particles from Dried Multilayer Polymer Capsules. *Biomacromolecules* **2013**, *14*, 3830−3841.
(33) Meng, H.; Yang, S.; Li, Z.; Xia, T.; Chen, J.; Ji, Z.; Zhang, H.; Wang, X.; Lin, S.; Huang, C.; Zhou, Z. H.; Zink, J. I.; Nel, A. E. Aspect Ratio Determines the Quantity of Mesoporous Silica Nanoparticle Uptake by a Small GTPase-Dependent Macropinocytosis Mechanism. *ACS Nano* **2011**, *5*, 4434−4447.
(34) Bruckman, M. A.; Randolph, L. N.; Van Meter, A.; Hern, S.; Shoffstall, A. J.; Taurog, R. E.; Steinmetz, N. F. Biodistribution, Pharmacokinetics, and Blood Compatibility of Native and PEGylated Tobacco Mosaic Virus Nano-Rods and -Spheres in Mice. *Virology* **2014**, *449*, 163−173.
(35) Yoo, J. W.; Doshi, N.; Mitragotri, S. Endocytosis and Intracellular Distribution of PLGA Particles in Endothelial Cells: Effect of Particle Geometry. *Macromol. Rapid Commun.* **2010**, *31*, 142−148.
(36) Kozlovskaya, V.; Alexander, J. F.; Wang, Y.; Kuncewicz, T.; Liu, X.; Godin, B.; Kharlampieva, E. Internalization of Red Blood Cell-Mimicking Hydrogel Capsules with pH-Triggered Shape Responses. *ACS Nano* **2014**, *8*, 5725−5737.
(37) Kozlovskaya, V.; Wang, Y.; Higgins, W.; Chen, J.; Chen, Y.; Kharlampieva, E. pH-Triggered Shape Response of Cubical Ultrathin Hydrogel Capsules. *Soft Matter* **2012**, *8*, 9828−9839.
(38) Calvert, P. Hydrogels for Soft Machines. *Adv. Mater.* **2009**, *21*, 743−756.
(39) Xu, S. Q.; Nie, Z. H.; Seo, M.; Lewis, P.; Kumacheva, E.; Stone, H. A.; Garstecki, P.; Weibel, D. B.; Gitlin, I.; Whitesides, G. M. Generation of Monodisperse Particles by Using Microfluidics: Control over Size, Shape, and Composition. *Angew. Chem., Int. Ed.* **2005**, *44*, 724−728.
(40) Perry, J. L.; Herlihy, K. P.; Napier, M. E.; Desimone, J. M. PRINT: A Novel Platform Toward Shape and Size Specific Nanoparticle Theranostics. *Acc. Chem. Res.* **2011**, *44*, 990−998.
(41) Wang, Y.; Caruso, F. Template Synthesis of Stimuli-Responsive Nanoporous Polymer-Based Spheres via Sequential Assembly. *Chem. Mater.* **2006**, *18*, 4089−4100.
(42) Yan, Y.; Lai, Z. W.; Goode, R. J. A.; Cui, J.; Bacic, T.; Kamphuis, M. M. J.; Nice, E. C.; Caruso, F. Particles on the Move: Intracellular Trafficking and Asymmetric Mitotic Partitioning of Nanoporous Polymer Particles. *ACS Nano* **2013**, *7*, 5558−5567.
(43) Kozlovskaya, V.; Chen, J.; Tedjo, C.; Liang, X.; Campos-Gomez, J.; Oh, J.; Saeed, M.; Lungu, C. T.; Kharlampieva, E. pH-Responsive Hydrogel Cubes for Release of Doxorubicin in Cancer Cells. *J. Mater. Chem. B* **2014**, *2*, 2494−2507.
(44) Zelikin, A. N.; Quinn, J. F.; Caruso, F. Disulfide Cross-Linked Polymer Capsules: En Route to Biodeconstructible Systems. *Biomacromolecules* **2006**, *7*, 27−30.
(45) Demaurex, N. pH Homeostasis of Cellular Organelles. *News Physiol. Sci.* **2002**, *17*, 1−5.
(46) Danhier, F.; Feron, O.; Préat, V. To Exploit the Tumor Microenvironment: Passive and Active Tumor Targeting of Nanocarriers for Anti-Cancer Drug Delivery. *J. Controlled Release* **2010**, *148*, 135−146.
(47) Liang, X.; Kozlovskaya, V.; Chen, Y.; Zavgorodnya, O.; Kharlampieva, E. Thermosensitive Multilayer Hydrogels of Poly(N-vinylcaprolactam) as Nanothin Films and Shaped Capsules. *Chem. Mater.* **2012**, *24*, 3707−3719.
(48) Kharlampieva, E.; Erel-Unal, I.; Sukhishvili, S. A. Amphoteric Surface Hydrogels Derived from Hydrogen-Bonded Multilayers: Reversible Loading of Dyes and Macromolecules. *Langmuir* **2007**, *23*, 175−181.
(49) Kozlovskaya, V.; Zavgorodnya, O.; Wang, Y.; Ankner, J. F.; Kharlampieva, E. Tailoring Architecture of Nanothin Hydrogels: Effect of Layering on pH-Triggered Swelling. *ACS Macro Lett.* **2013**, *2*, 226−229.
(50) Kozlovskaya, V.; Shamaev, A.; Sukhishvili, S. A. Tuning Swelling pH and Permeability of Hydrogel Multilayer Capsules. *Soft Matter* **2008**, *4*, 1499−1507.
(51) Wang, Y.; Yu, A.; Caruso, F. Nanoporous Polyelectrolyte Spheres Prepared by Sequentially Coating Sacrificial Mesoporous Silica Spheres. *Angew. Chem., Int. Ed.* **2005**, *44*, 2888−2892.
(52) Ochs, C. J.; Such, G. K.; Yan, Y.; Koeverden, M. P. V.; Caruso, F. Biodegradable Click Capsules with Engineered Drug-Loaded Multilayers. *ACS Nano* **2010**, *4*, 1656−1663.

DOI: 10.1021/acsami.5b03360
ACS Appl. Mater. Interfaces 2015, 7, 13633−13644

(53) Maciel, D.; Figueira, P.; Xiao, S.; Hu, D.; Shi, X.; Rodrigues, J.; Tomás, H.; Li, Y. Redox-Responsive Alginate Nanogels with Enhanced Anticancer Cytotoxicity. *Biomacromolecules* **2013**, *14*, 3140−3146.
(54) Guo, X.; Shi, C. I.; Yang, G.; Wang, J.; Cai, Z.; Zhou, S. Dual-Responsive Polymer Micelles for Target-Cell-Specific Anticancer Drug Delivery. *Chem. Mater.* **2014**, *26*, 4405−4418.
(55) He, C.; Hu, Y. P.; Yin, L. C.; Tang, C.; Yin, C. H. Effects of Particle Size and Surface Charge on Cellular Uptake and Biodistribution of Polymeric Nanoparticles. *Biomaterials* **2010**, *31*, 3657−3666.
(56) Haag, R.; Kratz, F. Polymer Therapeutics: Concepts and Applications. *Angew. Chem., Int. Ed.* **2006**, *45*, 1198−1215.
(57) Ortiz, C.; Hadziioannou, G. Entropic Elasticity of Single Polymer Chains of Poly(methacrylic acid) Measured by Atomic Force Microscopy. *Macromolecules* **1999**, *32*, 780−787.
(58) Steinhilber, D.; Sisson, A. L.; Mangoldt, D.; Welker, P.; Licha, K.; Haag, R. Synthesis, Reductive Cleavage, and Cellular Interaction Studies of Biodegradable, Polyglycerol Nanogels. *Adv. Funct. Mater.* **2010**, *20*, 4133−4138.
(59) Yang, P.; Li, D.; Jin, S.; Ding, J.; Guo, J.; Shi, W. B.; Wang, C. C. Stimuli-Responsive Biodegradable Poly(methacrylic acid) Based Nanocapsules for Ultrasound Traced and Triggered Drug Delivery System. *Biomaterials* **2014**, *35*, 2079−2088.
(60) Shuai, X.; Ai, H.; Nasongkla, N.; Kim, S.; Gao, J. Micellar Carriers Based on Block Copolymers of Poly(q-caprolactone) and Poly(ethylene glycol) for Doxorubicin Delivery. *J. Controlled Release* **2004**, *98*, 415−426.
(61) Tapia, C.; Costa, E.; Moris, M.; Sapag-Hagar, J.; Valenzuela, F.; Basualto, C. Study of the Influence of the pH Media Dissolution, Degree of Polymerization, and Degree of Swelling of the Polymers on the Mechanism of Release of Diltiazem from Matrices Based on Mixtures of Chitosan/Alginate. *Drug Dev. Ind. Pharm.* **2002**, *28*, 217−224.
(62) Pogodin, S.; Baulin, V. A. Can a Carbon Nanotube Pierce through a Phospholipid Bilayer? *ACS Nano* **2010**, *4*, 5293−5300.
(63) Gao, H.; Shi, W.; Freund, L. B. Mechanics of Receptor-Mediated Endocytosis. *Proc. Natl. Acad. Sci. U. S. A.* **2005**, *102*, 9469−9474.
(64) Mao, Z. W.; Zhou, X. Y.; Gao, C. Y. Influence of Structure and Properties of Colloidal Biomaterials on Cellular Uptake and Cell Functions. *Biomater. Sci.* **2013**, *1*, 896−911.
(65) Dasgupta, S.; Auth, T.; Gompper, G. Shape and Orientation Matter for the Cellular Uptake of Nonspherical Particles. *Nano Lett.* **2014**, *14*, 687−693.

DOI: 10.1021/acsami.5b03360
ACS Appl. Mater. Interfaces 2015, 7, 13633−13644